Electronic Supplementary Material (ESI) for Environmental Science: Nano.

Electronic Supplementary Information

A Novel Nitrogen-Doped $KFeS_2$/C Composites for Efficient Removal of Cr(VI)

Qiaohong Su [a, d], Adnan Ali Khan [c], Zhi Su [d], Chen Tian [a], Xiaoqin Li [a], Jiahua Gu [a], Ting Zhang [a], Rashid Ahmad [c**], Xintai Su [a, b*], Zhang Lin [a, b]

[a] *School of Environment and Energy, Guangdong Provincial Key Laboratory of Solid Wastes Pollution Control and Recycling, South China University of Technology, Guangzhou, Guangdong 510006, China*

[b] *Sino-Singapore International Joint Research Institute (SSIJRI), Guangzhou 510000, China.*

[c] *Department of Chemistry, University of Malakand, Chakdara, Khyber Pakhtunkhwa, Pakistan*

[d] *College of Chemistry and Chemical Engineering, Xinjiang Normal University, Urumqi 830054, Xinjiang, China*

**Corresponding authors email address: suxintai827@163.com, rashmad@gmail.com (Rashid Ahmad)*

Analyses of the adsorption data

The equilibrium adsorption capacity (q_e, mg g^{-1}) was calculated by *Eq*. (1):

$$q_e = \frac{V \cdot (C_0 - C_e)}{m} \quad (1)$$

where C_0 (mg L^{-1}) and C_e (mg L^{-1}) represent the initial and equilibrium concentrations of Cr(VI) in solutions respectively, V (L) and m (g) represent volume and mass, respectively.

The study of adsorption kinetics is of great significance for the objective evaluation of Cr(VI) adsorption rate. The kinetics of adsorption of Cr(VI) on NSC-1.3 was analyzed by using pseudo-first-order and pseudo-second-order models, which were expressed as *Eq*. (2) and *Eq*. (3), respectively:[1]

$$log(q_e - q_t) = logq_e - \frac{tk_1}{2.3303} \quad (2)$$

$$\frac{t}{q_t} = \frac{1}{k_2 q_e^2} + \frac{t}{q_e} \quad (3)$$

where q_e (mg g^{-1}) and q_t (mg g^{-1}) represent the adsorption capacity at equilibrium and time t, respectively, k_1 (min^{-1}) and k_2 (g min^{-1} mg^{-1}) represent the corresponding rate constants, respectively.

In order to evaluate the adsorption capacity of NSC-1.3 for Cr(VI), the Langmuir and Freundlich isothermal adsorption model was used to fit the experimental data at three temperatures. The models were expressed as *Eq*. (4) and *Eq*. (5), respectively:[2]

$$\frac{C_e}{q_e} = \frac{1}{q_m K_L} + \frac{C_e}{q_m} \quad (4)$$

$$logq_e = \frac{1}{n} logC_e + logK_F \quad (5)$$

Where C_e (mg L^{-1}) represents the equilibrium concentration, and q_e (mg g^{-1}) and q_m (mg g^{-1}) represent the equilibrium adsorption capacity and the maximum adsorption capacity, respectively, K_L (L mg^{-1}) is Langmuir equilibrium constant, K_F (mg g^{-1}) represents an adsorption coefficient, and n is the index coefficient.

The study of thermodynamic parameters such as Gibbs free energy change (ΔG°), enthalpy (ΔH°), and entropy change (ΔS°) has profound significance to the specific adsorption process. These parameter values can be calculated by *Eq*. (6), *Eq*.(7) and *Eq*.(8), respectively:[3]

$$\Delta G^\circ = -RT\ln K_d \quad (6)$$

$$K_d = \frac{q_e}{C_e} \quad (7)$$

$$\ln K_d = \frac{\Delta S^\circ}{R} - \frac{\Delta H^\circ}{RT} \quad (8)$$

Where K_d is the thermodynamic equilibrium constant, R (8.314 J mol^{-1} K^{-1}) is the gas constant, and T (K) is the experimental temperature.

DFT simulation details

The density functional theory (DFT) was used for all calculations implemented in Dmol3 code.[4,5] The generalized-gradient approximation (GGA) of Perdew-Burke-Ernzerhof (PBE) functional[6] was utilized for all geometry optimization and electronic properties calculations. In intermolecular interactions long-range dispersion-correction was set by applying the Grimme's DFT-D correction.[7,8] Double numerical plus-polarization (DNP) basis set and DFT semicore pseudopotenitals (DSPPs) were used for all the calculations.[9] While The thermal smearing was set to 0.005 au while the basis set cutoff was set to 4.6 Å. The convergence tolerance for geometries optimization was set to 10^{-5} Ha, 0.001 Ha/ Å for the energy while 0.005 Å for force and displacement. The $KFeS_2$ structure was modeled according to the recently reported literature[10] which is depicted in Fig. S1. Then we selected single layer 1 x 5 x 1 non-periodic single layer to reduce the computational simulations cost and just to check the N doping effects on the $KFeS_2$ structure and there adsorption behaviors towards the Cr(VI).

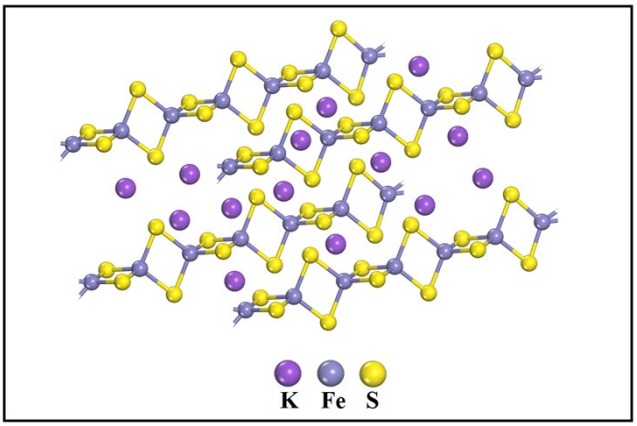

Fig. S1 Graphical representation of the $KFeS_2$ supercell structure.

The formation energy (E_f) for N doped system was calculated as:

$$E_f = E_{N\,KFeS_2} - (E_{n\,N} + E_{KFeS_2} - E_{nS}) \quad (9)$$

where, E_{NKFeS2} and E_{KFeS2} are the total energy of the N doped $KFeS_2$ layer and undoped $KFeS_2$ layer while the E_{nN} and E_{nS} are the total energies of the isolated N and S atoms, respectively. The adsorption energy (E_{ad}) was computed using the following equation:

$$E_{ad} = E_{complex} - (E_{M\,1} + E_{M\,2}) \quad (10)$$

here, $E_{complex}$ is the total energy of the complex system (H_2CrO_4 adsorbed over the pure or N doped $KFeS_2$ layer) while E_{M1} and E_{M2} are the total energy of the individual monomers (isolated pure $KFeS_2$, N-doped $KFeS_2$ layer and H_2CrO_4).

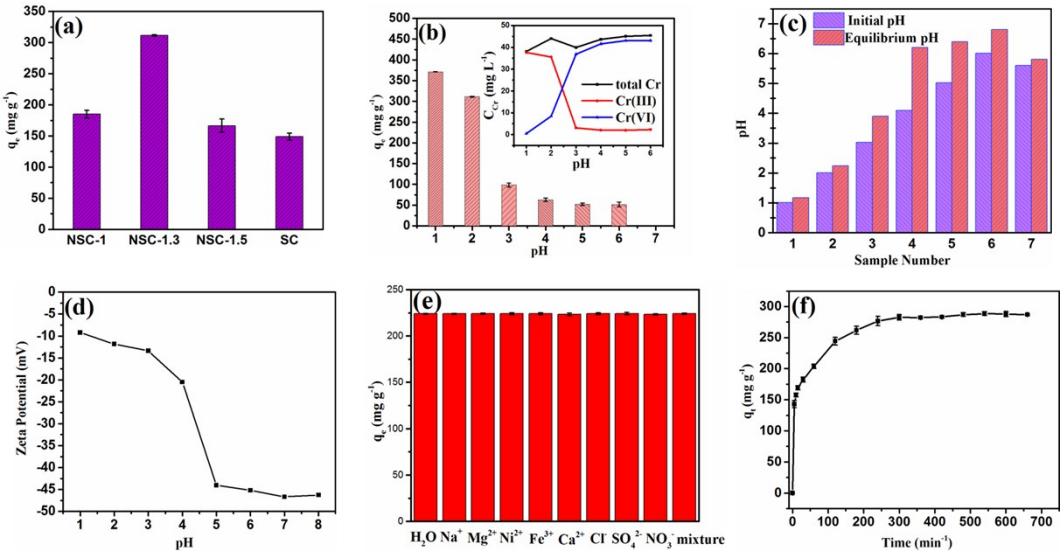

Fig. S2 (a) Adsorption properties of various adsorbents under the same conditions (m = 4 mg, V = 30 mL, T = 298 K, C_0 = 50 mg L^{-1}), (b) impact of pH values (m = 4 mg, V = 30 mL, T = 298 K, C_0 = 50 mg L^{-1}), the insertion diagram is chromium concentration at different pH conditions, (c) pH value changes before and after Cr(VI) adsorption, (d) Zeta potentials of NSC-1.3 in aqueous solution at different pH values, (e) impact of coexisting ions on Cr(VI) removal by NSC-1.3 (m = 4 mg, V = 30 mL, pH = 2, T = 298 K, C_0 = 30 mg L^{-1}), (f) impact of time on Cr(VI) removal by NSC-1.3 (m = 33.3 mg, V = 250 mL, pH = 2, T = 298 K, C_0 = 50 mg L^{-1}).

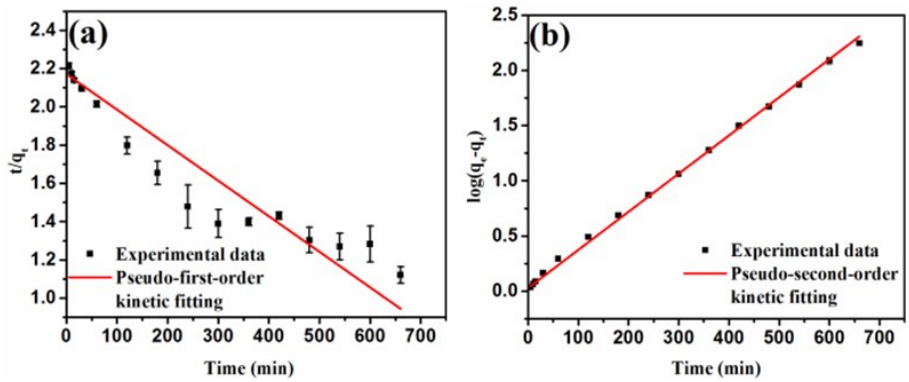

Fig. S3 (a) Pseudo first-order, (b) Pseudo second-order kinetic fitting of NSC-1.3 (m = 33.3 mg, V = 250 mL, pH = 2, T = 298 K, C_0 = 50 mg L^{-1}).

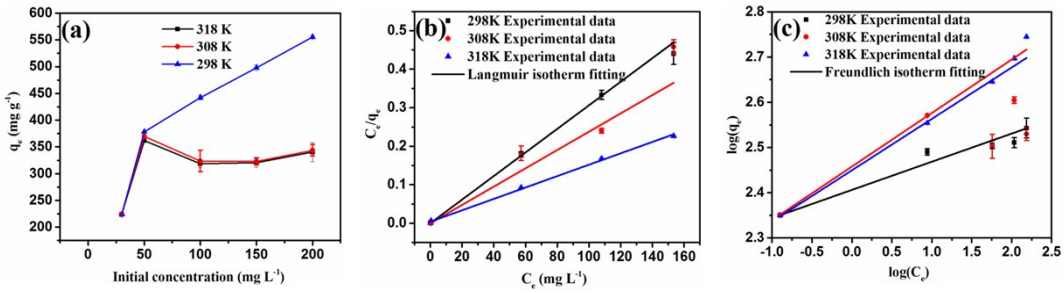

Fig. S4 (a) Effect of initial concentration and temperature, (b) Langmuir isotherm, (c) Freundlich isotherm fitting of NSC-1.3 at different temperatures (m = 4 mg, V = 30 mL, pH = 2, C_0 = 30 - 300 mg L^{-1}).

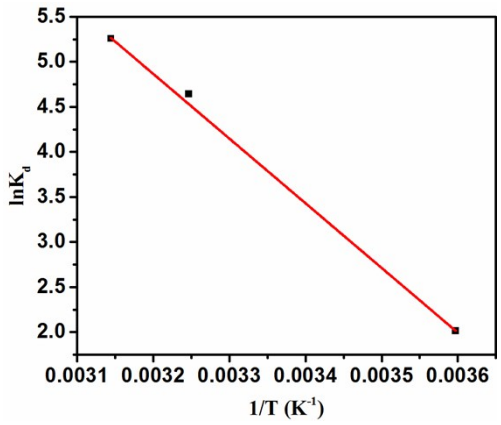

Fig. S5 Plot of lnK_d against 1/T for Cr(VI) removal on NSC-1.3 (m = 4 mg, V = 30 mL, pH = 2, C_0 = 50 mg L^{-1}, T = 298 - 318 K.

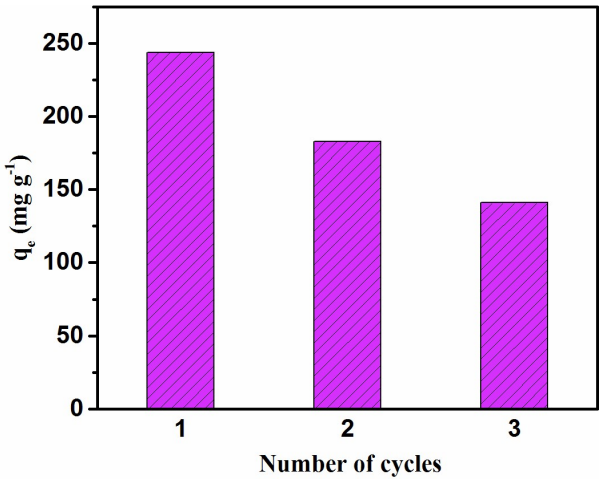

Fig. S6 Regeneration experiment of NSC-1.3 (pH = 2, C_0 = 50 mg L^{-1}, No. 1: m = 4 mg, V = 30 mL, No. 2: m = 2.7 mg, V = 20 mL, No. 3: m = 2 mg, V = 15 mL).

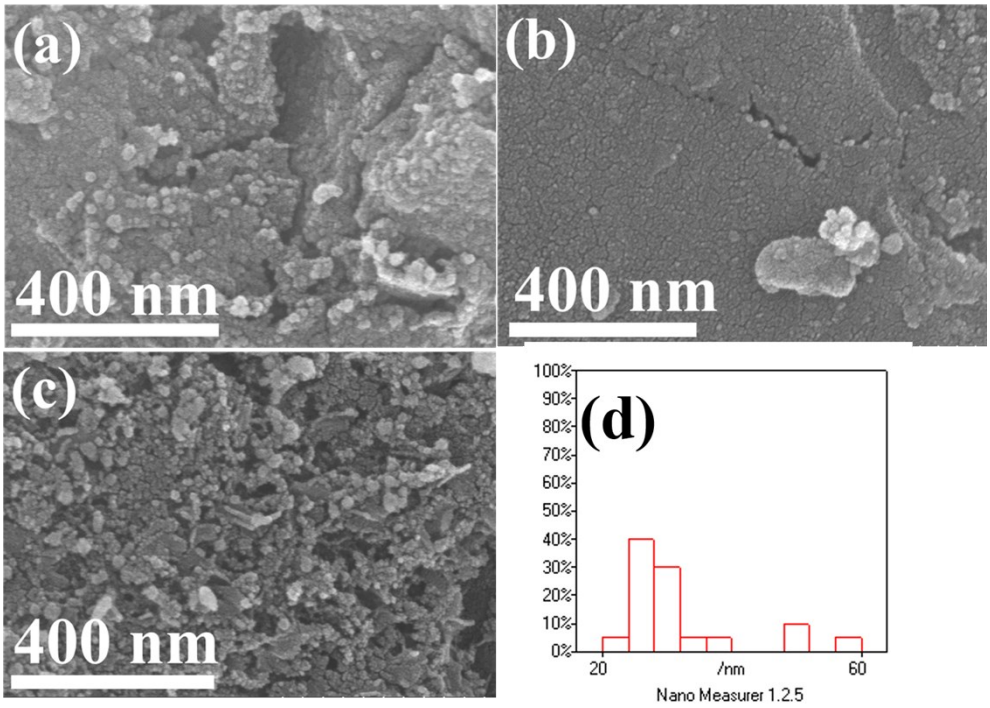

Fig. S7 (a) SEM image of primary NSC-1.3, (b) SEM image of NSC-1.3 after Cr(VI) adsorption, (c) SEM of NSC-1.3 after regeneration, (d) the diameter of nanoparticles from (c).

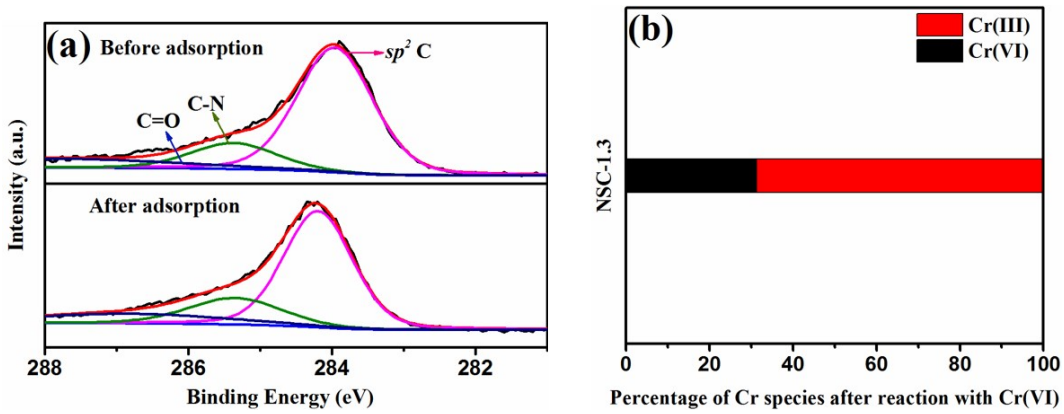

Fig. S8 (a) C 1s XPS spectra of NSC-1.3 before and after adsorption, (b) the percentage of Cr species after the reaction with Cr(VI).

Table S1 Comparison of removal properties of adsorbents for Cr(VI).

Absorbents	q_{max} (mg g^{-1})	pH	References
HAB-derived Fe/C	165.00	2	11
Fe/FeS	69.70	5	12
AMGO	123.40	2	13
NZVI/Fe_3O_4/graphene	101.00	3	14
Fe@PC	10.07	7	15
Corn cob-derived magnetic AC	125.00	2	16
Iron doped ordered mesoporous carbon	257.00	5	17
MAC-800	66.35	4	18
NDCS	432	3	19
N-doped carbon spheres	181.82	2	20
HA-N-MPC	130.5	2	21
N-doped porous carbon(Ni)	96.27	2.5	22
NSC-1.3	326.80	2	This work

Table S2 Thermodynamic parameters of Cr(VI) removal on NSC-1.3.

ΔH° (kJ mol^{-1})	ΔS° (J mol^{-1} K^{-1})	ΔG° (kJ mol^{-1})		
		298 K	308 K	318 K
59.6868	231.4532	-9.2863	-11.6088	-13.9153

Table S3 The content of different chemical states of N 1s and S 2p in NSC-1.3

	Sulphur content (%)				Nitrogen content (%)					
	Total	S_n^{2-}	S_8	S(VI)	Total	N(I)	N(II)	N(III)	N(IV)	N(V)
Before adsorption	8.5	45.1	31.8	23.1	3.01	19.9	19.9	20.0	20.1	20.1
After	7.1	39.5	28.1	32.4	2.98	33.9	11.2	28.9	18.3	7.7

References

1 M. Taghizadeh and S. Hassanpour, Selective adsorption of Cr(VI) ions from aqueous solutions using a Cr(VI)-imprinted polymer supported by magnetic multiwall carbon nanotubes, *Polym.*, 2017, **132**, 1-11.

2 K. Gong, Q. Hu, L. Yao, M. Li, D. Sun, Q. Shao, B. Qiu and Z. Guo, Ultrasonic pretreated sludge derived stable magnetic active carbon for Cr(VI) removal from wastewater, *ACS Sustain. Chem. Eng.*, 2018, **6**, 7283-7291.

3 F. Liu, X. Wang, B. Chen, S. Zhou and C. Chang, Removal of Cr(VI) using polyacrylonitrile/ferrous chloride composite nanofibers, *J. Taiwan Inst Chem Eng.*, 2017, **70**, 401-410.

4 B. Delley, An all-electron numerical method for solving the local density functional or polyatomic molecules, *J. Chem. Phys.*, 1990, **92**, 508–517.

5 B. Delley, from molecules to solids with the DMol3 approach, *J. Chem. Phys.*, 2000, **113**, 7756–7764.

6 J.P. Perdew, K. Burke and M. Ernzerhof, Generalized gradient approximation made simple, *Phys. Rev. Lett.*, 1996, **77**, 3865–3868.

7 S. Grimme, Accurate description of van der Waals complexes by density functional theory including empirical corrections, *J. Comput. Chem.*, 2004, **25**, 1463–1473.

8 S. Grimme, Semiempirical GGA-type density functional constructed with a long range dispersion correction, *J. Comput. Chem.*, 2006, **27**, 1787–1799.

9 P. Liu and J. Rodriguez, Catalysts for hydrogen evolution from the [NiFe] hydrogenase to the Ni_2P (001) surface: the importance of ensemble effect, *J. Am. Chem. Soc.*, 2005, **127**, 14871–14878.

10 B. Vaccaro, S. Clarkson, J. Holden, D. Lee, C. Wu, F. Poole and H. Li, Biological iron-sulfur storage in a thioferrate-protein nanoparticle, *Nat. Commun.*, 2017, **8**, 1-9.

11 Y. Cui, H. He and J. D. Atkinson, Iron/Carbon Composites for Cr(VI) removal prepared from harmful algal bloom biomass via metal bioaccumulation or biosorption, *ACS Sustain. Chem. Eng.*, 2018, **7**, 1279-1288.

12 Y. Gong, L. Gai, J. Tang and J. Fu, Reduction of Cr(VI) in simulated groundwater by FeS-coated iron magnetic nanoparticles, *Sci. Total Environ.*, 2017, **595**, 743-751.

13 D. Zhao, X. Gao, C. Wu and R. Xie, Facile preparation of amino functionalized graphene oxide decorated with Fe_3O_4 nanoparticles for the adsorption of Cr(VI), *Appl. Surf. Sci.*, 2016, **384**, 1-9.

14 X. Lv, X. Xue, G. Jiang, D. Wu, T. Sheng, H. Zhou and X. Xu, Nanoscale zero-valent iron (nZVI) assembled on magnetic Fe_3O_4/graphene for Chromium(VI) removal from aqueous solution, *J. Colloid Interface Sci.*, 2014,**417**, 51-59.

15 L. Zhuang, Q. Li, J. Chen, B. Ma and S. Chen, Carbothermal preparation of porous carbon-encapsulated iron composite for the removal of trace hexavalent chromium, *Chem. Eng. J.*, 2014, **253**, 24-33.

16 S. Nethaji, A. Sivasamy and A. B. Mandal, Preparation and characterization of corn cob activated carbon coated with nano-sized magnetite particles for the removal of Cr(VI), *Bioresour. Technol.*, 2013, **134**, 94-100.

17 L. Tang, G. Yang, G. Zeng, Y. Cai, S. Li, Y. Zhou, Y. Pang, Y. Liu, Y. Zhang and B. Luna, Synergistic effect of iron doped ordered mesoporous carbon on adsorption-coupled reduction of hexavalent chromium and the relative mechanism study, *Chem. Eng. J.*, 2014, **239**, 114-122.

18 C. Demarchi, B. Michel, N. Nedelko, A. Ślawska-Waniewska, P. Dłużewski, A. Kaleta, R. Minikayev, T. Strachowski, L. Lipińska, J. Magro and C. Rodrigues, Preparation, characterization, and application of magnetic activated carbon from termite feces for the adsorption of Cr(VI) from aqueous solutions, *Powder Technol.*, 2019, **354**, 432-441.

19 I. Hussain, J. Qi, X. Sun, L. Wang, J. Li, Melamine derived nitrogen-doped carbon sheet for the efficient removal of chromium(VI), J. Mol. Liq., 2020, 318.

20 J. Wei , W. Cai, One-step hydrothermal preparation of N-doped carbon spheres from peanut hull for efficient removal of Cr(VI), J. Environ. Chem. Eng., 2020, 8, 104449.

21 T. Zhang, S. Wei, G. Waterhouse, L. Fu, L. Liu, W. Shi, J. Sun, S. Ai, Chromium(VI) adsorption and reduction by humic acid coated nitrogen-doped magnetic porous carbon, Powder Technol., 2019, 360.

22 S. Zhang, X. Wang, J. Li, T. Wen, J. Xu, X. Wang, Efficient removal of a typical dye

and Cr(VI) reduction using N-doped magnetic porous carbon, RSC Adv., 2014, 4, 63110-7.